

# On the Weak Binding and Spectroscopic Signature of SARS-CoV-2 nsp14 Interaction with RNA

Ayaz Hassan,<sup>[a]</sup> Graziela C. Sedenho,<sup>[a]</sup> Phelipe A. M. Vitale,<sup>[b]</sup> Mona N. Oliveira,<sup>[b]</sup> and Frank N. Crespilho<sup>\*[a]</sup>

The SARS-CoV-2 non-structural protein 14 (nsp14), known as exoribonuclease is encoded from the large polyprotein of viral genome and is a major constituent of the transcription replication complex (TRC) machinery of the viral RNA synthesis. This protein is highly conserved among the coronaviruses and is a potential target for the development of a therapeutic drug. Here, we report the SARS-CoV-2 nsp14 expression, show its structural characterization, and ss-RNA exonuclease activity through vibrational and electronic spectroscopies. The deconvolution of amide-I band in the FTIR spectrum of the protein revealed a composition of 35%  $\alpha$ -helix and 25%  $\beta$ -sheets. The binding between protein and RNA is evidenced from the spectral changes in the amide-I region of the nsp14, showing protein conformational changes during the binding process. A value of  $20.60 \pm 3.81 \text{ mol L}^{-1}$  of the binding constant ( $K_D$ ) is obtained for nsp14/RNA complex. The findings reported here can motivate further studies to develop structural models for better understanding the mechanism of exonuclease enzymes for correcting the viral genome and can help in the development of drugs against SARS-CoV-2.


After outbreak of second severe acute respiratory syndrome coronavirus (SARS-CoV-2), much molecular level information has been published providing the detailed structural analysis of SARS-CoV-2 genome, which is almost similar to SARS-CoV with few differences in the accessory proteins.<sup>[1]</sup> SARS-CoV-2 genome is a positive-strand RNA of approximately 30 Kb, the largest of all known coronaviruses recognized so far.<sup>[2,3]</sup> The replication fidelity rate of most of the coronaviruses, including SARS-CoV-2, typically ranges from  $10^{-6}$  to  $10^{-7}$ ,<sup>[4]</sup> which is about  $10^{-2}$  to  $10^{-3}$  order of magnitude more accurate as compared to other RNA viruses.<sup>[5]</sup> Such a high-fidelity rate of SARS-CoV genome is maintained because of the exonuclease activity of the non-structural protein 14 (nsp14) of these viruses, which acts as a proofreading site in the transcription replication complex

(TRC).<sup>[6]</sup> This enzyme avoids the occurrence of any error in the viral RNA during the synthesis process, thus keeps the replication cycle highly accurate.<sup>[7]</sup> The structure of SARS-CoV-2 nsp14 protein is composed of two functional domains: exonuclease (ExoN) domain and N-7 methyltransferase (N7-MTase) domain.<sup>[8]</sup> Each domain has distinct function, which is functionally independent and structurally dependent on each other. While the ExoN domain is responsible for the proofreading of the newly synthesized RNA, the N7-MTase domain plays a major role in the messenger RNA (mRNA) capping. The specific arrangement of secondary structure elements makes the ExoN domain similar to the structure of other exonucleases of DEDDh superfamily e.g., DNA polymerase I and III from *Escherichia coli* (*E. coli*).<sup>[9]</sup> The DEDDh exonucleases follow a similar mechanism of catalysis, assisted by two metal ions and one water molecule to remove the misincorporated nucleotides.<sup>[10]</sup> The ExoN domain of nsp14 has been reported to exhibit an exonuclease activity from 3' to 5' direction of nucleic acids, functioning as proofreading site by excising nucleoside monophosphate.<sup>[11]</sup> The ExoN activity of nsp14 is orchestrated by five conserved active sites residues that are arranged over three canonical motifs.<sup>[12]</sup> The exonuclease activity of nsp14 from SARS-CoV was first reported *in vitro* through biochemical analysis using different synthetic RNA strands as substrates.<sup>[13]</sup> Since then, several studies have been reported revealing that disrupting the activity of ExoN domain of nsp14 through inactivation or mutagenesis of active sites residues decreases the replication fidelity of the CoVs.<sup>[7,14]</sup> Therefore, investigating the nsp14 as a target for the drug development seems to be an effective strategy against the current Covid-19 pandemic and any future similar outbreaks. Previous studies on SARS-CoV and SARS-CoV-2 nsp14 and their interactions with RNA substrates have been limited only to biochemical analysis, such as gel-electrophoresis,<sup>[4,7]</sup> which requires complex sampling procedure, labelling, and expensive detection methods.

Fourier transform infrared (FTIR) spectroscopy on the other hand is a fast, simple and label-free technique, and has a great potential in analyzing the biological samples, particularly the proteins and the nucleic acids,<sup>[15,16]</sup> because of the vibrational signatures of these molecules and has been extensively exploited for taking a detailed information of these molecules and their interaction. Most importantly, the binding of the proteins with the DNA/RNA occurs *via* the electrostatic interaction between the polypeptide chain and the phosphate backbone of the nucleic acids,<sup>[17,18]</sup> which could be observed from the changes in the vibrational modes characteristic to these structures. Therefore, the IR spectroscopy provides useful

[a] Dr. A. Hassan, Dr. G. C. Sedenho, Prof. F. N. Crespilho  
Department of Physical Chemistry,  
São Carlos Institute of Chemistry, University of São Paulo  
Av. Trabalhador São Carlense, 400 – Parque Arnold Schmidt  
São Carlos – SP, 13566-590 (Brazil)  
E-mail: frankcrespilho@iqsc.usp.br

[b] P. A. M. Vitale, M. N. Oliveira  
Biolinker, Av. Prof. Lineu Prestes  
Cietec – Butantã, São Paulo, SP, 05508-000 (Brazil)

 Supporting information for this article is available on the WWW under <https://doi.org/10.1002/cbic.202100486>

insights into the proteins and oligonucleotides structures, being a suitable alternative for characterization of SARS-CoV-2 nsp14 protein and investigation of its molecular interaction with the RNA substrates for better understanding the mechanism behind this process.

Here, we report the SARS-CoV-2 nsp14 expression and purification protocol<sup>[19]</sup> (Supporting information, S-1 and S-2) and provide the spectroscopic data on the structural analysis of nsp14 in the isolated form and its interaction with RNA substrate in aqueous solution. As a further support to the traditional biochemical characterization of the nsp14/RNA complex formation *in vitro* and in the drug development process, we propose a new micro-FTIR spectroscopy assay that provides fundamental understanding of the major important biomolecular interaction process. For this, we report the structural analysis of SARS-CoV-2 nsp14 protein and RNA through multiplexed micro-FTIR spectroscopy. Additionally, we show the interaction of protein with the RNA under physiological conditions and support our results by calculating the binding constant ( $K_D$ ) of the nsp14/RNA complex formation through UV-Vis spectroscopy.

FTIR spectroscopy has shown an important role in the determination of protein secondary structure, protein conformational analysis, and structural characterization of nucleic acids. Particularly in the mid-infrared (MIR) region (i.e., from 4000 to 700  $\text{cm}^{-1}$ ) of the IR spectrum, both proteins and nucleic acids exhibit well-defined IR bands due to the presence of defining features present in the structures of these molecules, such as amide-I and amide-II bands of proteins and phosphate backbone bands of nucleic acids.<sup>[20]</sup> As micro-FTIR spectroscopy enables the data collection from minute amount of sample ( $\sim 2 \mu\text{L}$ ) supported on gold coated glass mirror with enhanced sensitivity, we used this technique for analyzing our samples. A small amount ( $2 \mu\text{L}$ ) of the nsp14 and RNA sample solutions were drop-cast on a gold-coated glass substrate and dried at room temperature for about 30 minutes, resulting in the formation of thin films (see supporting information S-4 and Figure S2 for further details).

Micro-FTIR spectroscopic measurements were performed by averaging 256 spectra, which were collected from 4096 different points of the probing sample with a spatial resolution of  $2.5 \mu\text{m}$ . Figure 1a shows the micro-FTIR spectra of nsp14 and RNA exhibiting the characteristic vibrational bands of protein and nucleic acids (for the detail assignment of the bands observed in the FTIR spectra, see Table S1, Table S2). For the nsp14, the main bands are observed at 1665 and 1550  $\text{cm}^{-1}$ , which are the principle vibrational modes of the protein structure and are assigned as amide-I and amide-II bands, respectively. The third most important band is attributed to amide-III, which is observed at 1245  $\text{cm}^{-1}$ . Besides, the other bands observed at 1448, 1320, and 1080  $\text{cm}^{-1}$  correspond to the CH deformation,  $\text{CH}_2$  wagging, and C–C stretching vibrational modes, respectively. On the other hand, in the RNA spectrum, the main vibrational modes, 1710, 1645, 1600, and 1480  $\text{cm}^{-1}$  correspond to the C=O stretching, C=C stretching mode of uracil, C=N stretching mode of adenine, and C–H deformation mode, respectively.<sup>[18,21]</sup> Similarly, the fingerprint

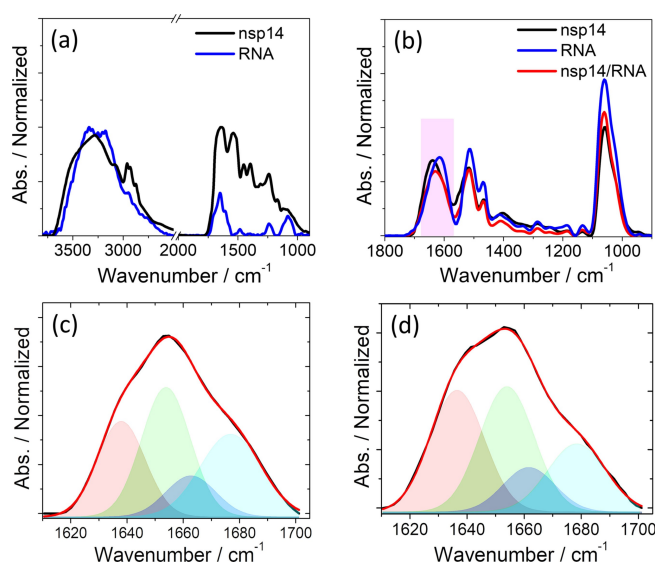


**Figure 1.** Micro-FTIR spectroscopy of nsp14, RNA, and nsp14/RNA complex: (a) micro-FTIR spectra of nsp14 and RNA films immobilized on Au-coated glass substrate, (b) micro-FTIR spectra of nsp14, RNA, and nsp14/RNA complex films immobilized on Au-coated glass substrate (the FTIR spectra shown in panel (a) are of the dialyzed samples solution, whereas the spectra recorded in panel (b) are of buffered samples solution), (c) deconvoluted amide-I band of nsp14 for obtaining secondary structure elements of protein, and (d) deconvoluted amide-I band of nsp14/RNA complex for obtaining secondary structure elements of the protein. The red lines in panels (c) and (d) represent the sum of the fits from all individual contributions.

vibrational modes of oligonucleotide (i.e., symmetric and asymmetric stretching modes of  $\text{PO}_2^-$ ) were observed at 1240 and 1080  $\text{cm}^{-1}$ , respectively. The chemical images are obtained by the integration of the amide-I band and phosphate backbone band in the micro-FTIR spectra for nsp14 and RNA, respectively, showing the distribution of these spectral bands and hence of the samples along the probed areas of the sample films (Supporting information, S-5).

Next, we show the interaction between nsp14 and RNA through measurement of micro-FTIR spectra, recorded for nsp14, RNA, and nsp14/RNA complex (Figure 1b). Evidence for complexation comes from the changes observed in the spectral bands of protein after interaction with RNA. The change is more pronounced in the amide-I (highlighted), where this band shifts to a lower wavenumber from 1640 to 1630  $\text{cm}^{-1}$ . The amide-I being a hybrid band of C=O and C–N groups stretching, which are the main components of the protein polypeptide chain, the results suggest that the molecular interaction between the exonuclease and RNA substrate occurs *via* hydrogen bonding from the polypeptide matrix. Besides, these spectral changes also propose a change in the protein conformation after complexation. Further insight into the nsp14-RNA interaction comes from the protein conformational analysis before and after complexation. For this the nsp14 secondary structure elements were obtained by the deconvolution of amide-I band (i.e., from 1700 to 1610  $\text{cm}^{-1}$ ) according to the second derivative method<sup>[22]</sup> and the bands were assigned as reported elsewhere.<sup>[23]</sup> The results showed that nsp14 is composed of

35%  $\alpha$ -helix and 25%  $\beta$ -sheets (Figure 1c), which is consistent to the protein crystal structure data.<sup>[8]</sup> The comparison of the secondary structure elements obtained from the deconvolution of amide-I with that from protein data bank (PDB) is shown in Table S3. However, some alteration in secondary structure elements of protein was noticed after the nsp14/RNA complex formation (Figure 1d). A major change (from 25% to 33%) was observed in  $\beta$ -sheets, with an associated decrease in the random coils (from 27% to 19%), suggesting a partial unfolding of protein during the binding and proof-reading process. These results show that the protein undergoes structural change to form the active catalytic site before it interacts with the RNA for the removal of mismatched nucleotides.

The UV-Vis absorption spectra of free RNA, nsp14, and nsp14/RNA complex are shown in Figure 2a. The absorption spectra of nsp14 and RNA show the characteristic absorption bands at approximately 280 and 260 nm, corresponding to  $\pi$ - $\pi^*$  transition of aromatic amino acids residues (Trp and Tyr) and guanine nucleobases, respectively. However, the spectrum of nsp14-RNA exhibits combined features from both protein and RNA, particularly the newly developed band at 230 nm (highlighted), corresponding to transition from peptide group of main chain. The nsp14/RNA binding constant was calculated through UV-Vis absorption spectroscopy by measuring the absorption of the complexes formed from the different protein concentration and constant oligonucleotide concentration (Figure 2b and supporting information S6). For this an experimental plot was constructed by using the Benesi-Hildebrand method, as described Equation (1).<sup>[24]</sup>

$$\frac{1}{A - A_0} = \frac{1}{A_f - A_0} + \frac{1}{K_b [C_{Ligand}] (A_f - A_0)} \quad (1)$$

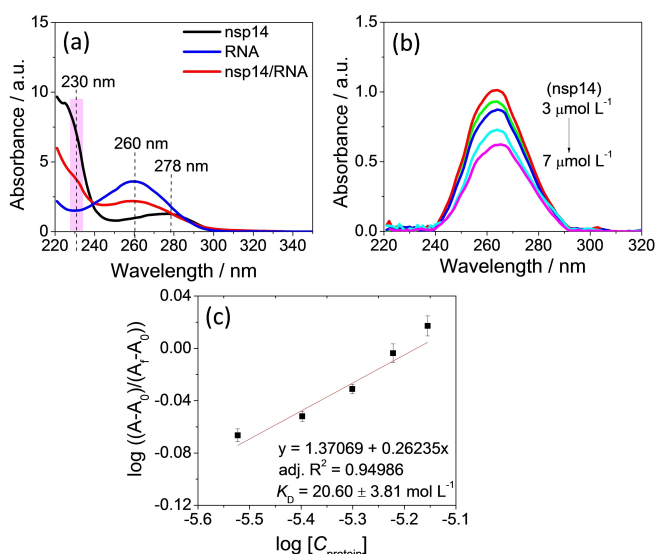


**Figure 2.** UV-Vis absorption spectroscopy of nsp14, RNA, and nsp14/RNA complex: (a) UV-Vis spectra of nsp14, RNA, and nsp14/RNA complex, (b) UV-Vis spectra of nsp14/RNA complexes with constant RNA and varying protein concentration, and (c) Benesi-Hildebrand plot for the binding constant ( $K_D$ ) determination of nsp14/RNA complex. The absorbance was measured in triplicate for each protein/RNA complex.

After rearrangement and replacing  $C_{ligand}$  by  $C_{protein}$  we obtained Equation (2):

$$\log \frac{A - A_0}{A_f - A_0} = \log [C_{protein}] + \log K_b \quad (2)$$

A value of  $20.60 \pm 3.81 \text{ mol L}^{-1}$  of the  $K_D$  was obtained for nsp14/RNA complex by linear fitting the experimental data to equation 2 (Figure 2c), which is considerably lower than the values previously reported for the RNA complexes with other proteins.<sup>[18]</sup> The low value of  $K_D$  of nsp14/RNA complex is attributed to the lower activity of nsp14 due to the absence of nsp10 protein, which improves the activity of nsp14 by several folds by acting as co-factor of nsp14.<sup>[25]</sup>

In summary, we have provided the SARS-CoV-2 non-structural nsp14 expression protocol and a structural spectroscopic characterization toward nsp14 and RNA binding. Weak binding and spectroscopic signature of SARS-CoV-2 nsp14 protein interaction with RNA are presented. For better understanding the genome editing process, it is important to biochemically characterize this protein in the presence and absence of RNA substrates. Some studies are reported in the literature,<sup>[4,5,26]</sup> providing the detailed structural information of nsp14 and its exonuclease activity. They are related to traditional biochemical analysis showing no efforts for understanding the mechanism of the binding and proofreading process. In another way, here we adopt an approach by using micro-FTIR spectroscopy, an easy-to-handle characterization and investigation tool of biological molecules to study nsp14 and its exonuclease activity in the presence of RNA substrate. The excessively large genome of coronaviruses puts a burden on these viruses because the viral genome can incur errors during the replication process. Therefore, it is necessary for the coronaviruses to develop a mechanism to guarantee the error-free progeny. The SARS-CoV and SARS-CoV-2 nsp14 protein is believed to involve in the proof-reading of the nascent RNA, because of its structural similarities to other exonucleases, such as DNA polymerase.

By using micro-FTIR spectroscopy protocol, we have shown the basic structural components of both nsp14 and RNA molecules and changes in the protein conformation upon binding to RNA. The secondary structure elements obtained *via* the deconvolution of the amide-I band are in close agreement to the protein crystal structure data. The spectral changes observed in the micro-FTIR spectrum of nsp14/RNA complex as compared to individual spectra, revealed that protein undergoes structural changes upon binding to RNA. UV-Vis spectroscopy showed the defining absorption bands of both nsp14 and RNA and appearance of extra bands in their binary complex, conforming that the interaction occurs through the polypeptide chain. Based on the results obtained from micro-FTIR and UV-Vis spectroscopy, it is inferred that protein undergoes conformational change upon RNA binding, which is considered as an important process for the catalytic activity of protein. Though a detailed mechanism of the catalytic process of nsp14 for removing the uncorrected nucleobases from the viral genome during the replication process still to be

developed, our study can provide a fundamental step in this direction.

## Acknowledgements

The authors gratefully acknowledge the São Paulo Research Foundation (FAPESP) for the financial support of the research projects under the grant numbers: 19/15333-1, 19/12053-8, 18/22214-6 and 2020/04796-8, Coordinating Agency for Advanced Training of Graduate Personnel (CAPES), MeDiCo Network CAPES Brazil grant number 88881.504532/2020-01 and CAPES-PNPD grant number 88887.358060/2019-00 and National Council of Scientific and Technological Development (CNPq) grant number 305486/2019-5. The authors thank the Ph.D. student Ms. Amanda Imamura from BioMicS Group (São Carlos Institute of Chemistry, University of São Paulo) for providing the technical support in performing the UV-Vis spectroscopic analysis.

## Conflict of Interest

The authors declare no conflict of interest.

**Keywords:** micro-FTIR spectroscopy · non-structural proteins · nsp14 · RNA · SARS-CoV-2

- [1] D. E. Gordon, G. M. Jang, M. Bouhaddou, J. Xu, K. Obernier, K. M. White, M. J. O'Meara, V. V. Rezell, J. Z. Guo, D. L. Swaney, T. A. Tummino, R. Hüttenhain, R. M. Kaake, A. L. Richards, B. Tutuncuoglu, H. Foussard, J. Batra, K. Haas, M. Modak, M. Kim, P. Haas, B. J. Polacco, H. Braberg, J. M. Fabius, M. Eckhardt, M. Souchery, M. J. Bennett, M. Cakir, M. J. McGregor, Q. Li, B. Meyer, F. Roesch, T. Vallet, A. Mac Kain, L. Miorin, E. Moreno, Z. Z. C. Naing, Y. Zhou, S. Peng, Y. Shi, Z. Zhang, W. Shen, I. T. Kirby, J. E. Melnyk, J. S. Chorba, K. Lou, S. A. Dai, I. Barrio-Hernandez, D. Memon, C. Hernandez-Armenta, J. Lyu, C. J. P. Mathy, T. Perica, K. B. Pilla, S. J. Ganesan, D. J. Saltzberg, R. Rakesh, X. Liu, S. B. Rosenthal, L. Calviello, S. Venkataramanan, J. Liboy-Lugo, Y. Lin, X. P. Huang, Y. F. Liu, S. A. Wankowicz, M. Bohn, M. Safari, F. S. Ugur, C. Koh, N. S. Savar, Q. D. Tran, D. Shengjuler, S. J. Fletcher, M. C. O'Neal, Y. Cai, J. C. J. Chang, D. J. Broadhurst, S. Klippsten, P. P. Sharp, N. A. Wenzell, D. Kuzuoglu-Ozturk, H. Y. Wang, R. Trenker, J. M. Young, D. A. Caverio, J. Hiatt, T. L. Roth, U. Rathore, A. Subramanian, J. Noack, M. Hubert, R. M. Stroud, A. D. Frankel, O. S. Rosenberg, K. A. Verba, D. A. Agard, M. Ott, M. Emerman, N. Jura, M. von Zastrow, E. Verdin, A. Ashworth, O. Schwartz, C. d'Enfert, S. Mukherjee, M. Jacobson, H. S. Malik, D. G. Fujimori, T. Ideker, C. S. Craik, S. N. Floor, J. S. Fraser, J. D. Gross, A. Sali, B. L. Roth, D. Ruggero, J. Taunton, T. Kortemme, P. Beltrao, M. Vignuzzi, A. Garcia-Sastre, K. M. Shokat, B. K. Shoichet, N. J. Krogan, *Nature* **2020**, *583*, 459–468.
- [2] F. A. Rabi, M. S. Al Zoubi, G. A. Kasasbeh, D. M. Salameh, A. D. Al-nasser, *Pathogenesis* **2020**, *231*, 1–14.
- [3] S. Srinivasan, H. Cui, Z. Gao, M. Liu, S. Lu, W. Mkandawire, O. Narykov, M. Sun, D. Korkin, *Viruses* **2020**, *12*, 1–17.
- [4] H. T. Baddock, S. Brolih, Y. Yosaatmadja, M. Ratnaweera, M. Bielinski, L. P. Swift, A. Cruz-Migoni, G. M. Morris, C. J. Schofield, O. Gileadi, P. J. Mchugh, *bioRxiv* **2020**, <https://www.biorxiv.org/content/10.1101/2020.08.13.248211v1>.
- [5] M. Sevajol, L. Subissi, E. Decroly, B. Canard, I. Imbert, *Virus Res.* **2014**, *194*, 90–99.
- [6] E. Minskaia, T. Hertzog, A. E. Gorbalenya, V. Campanacci, C. Cambillau, B. Canard, J. Ziebuhr, *Proc. Natl. Acad. Sci. USA* **2006**, *103*, 5108–5113.
- [7] N. S. Ogando, J. C. Zevenhoven-Dobbe, Y. van der Meer, P. J. Bredenbeek, C. C. Posthuma, E. J. Snijder, *J. Virol.* **2020**, *94*, 1–24.
- [8] Y. Ma, L. Wu, N. Shaw, Y. Gao, J. Wang, Y. Sun, Z. Lou, L. Yan, R. Zhang, Z. Rao, *Proc. Natl. Acad. Sci. USA* **2015**, *112*, 9436–9441.
- [9] S. Hamdan, P. D. Carr, S. E. Brown, D. L. Ollis, N. E. Dixon, *Structure* **2002**, *10*, 535–546.
- [10] L. S. Beese, T. A. Steitz, *EMBO J.* **1991**, *10*, 25–33.
- [11] J. Meador, B. Cannon, V. J. Cannistraro, D. Kennel, *Eur. J. Biochem.* **1990**, *187*, 549–553.
- [12] F. Robson, K. S. Khan, T. K. Le, C. Paris, S. Demirbag, P. Barfuss, P. Rocchi, W. L. Ng, *Mol. Cell* **2020**, *79*, 710–727.
- [13] M. R. Denison, R. L. Graham, E. F. Donaldson, L. D. Eckerle, R. S. Baric, *RNA Biol.* **1992**, *120*, 215–218.
- [14] M. Bouvet, I. Imbert, L. Subissi, L. Gluais, B. Canard, E. Decroly, *Proc. Natl. Acad. Sci. USA* **2012**, *109*, 9372–9377.
- [15] A. Barth, *Biochim. Biophys. Acta* **2007**, *1767*, 1073–1101.
- [16] J. Kong, S. Yu, *Acta Biochim. Biophys. Sin.* **2007**, *39*, 549–559.
- [17] A. Hassan, L. J. A. Macedo, J. C. P. de Souza, F. C. D. A. Lima, F. N. Crespilho, *Sci. Rep.* **2020**, *10*, 1931.
- [18] H. A. Tajmiri-Riahi, C. N. N'soukpoe-Kossi, D. Joly, *Spectroscopy* **2009**, *23*, 81–101.
- [19] N. Altincekic, S. M. Korn, N. S. Qureshi, M. Dujardin, M. Ninot-Pedrosa, R. Abele, M. J. Abi Saad, C. Alfano, F. C. L. Almeida, I. Alshamleh, G. C. de Amorim, T. K. Anderson, C. D. Anobom, C. Anorma, J. K. Bains, A. Bax, M. Blackledge, J. Blechar, A. Böckmann, L. Brigandat, A. Bula, M. Bütikofer, A. R. Camacho-Zarco, T. Carlomagno, I. P. Caruso, B. Ceylan, A. Chaikvad, F. Chu, L. Cole, M. G. Crosby, V. de Jesus, K. Dhamotharan, I. C. Felli, J. Ferner, Y. Fleischmann, M. L. Fogeron, N. K. Fourkiotis, C. Fuks, B. Fürtig, A. Gallo, S. L. Gande, J. A. Gerez, D. Ghosh, F. Gomes-Neto, O. Gorbatyuk, S. Guseva, C. Hacker, S. Häfner, B. Hao, B. Hargittay, K. Henzler-Wildman, J. C. Hoch, K. F. Hohmann, M. T. Hutchison, K. Jaudzems, K. Jović, J. Kaderli, G. Kalniņš, I. Kaņepe, R. N. Kirchdoerfer, J. Kirkpatrick, S. Knapp, R. Krishnathas, F. Kutz, S. zur Lage, R. Lambert, A. Lang, D. Laurents, L. Lecoq, V. Linhard, F. Löhr, A. Malki, L. M. Bessa, R. W. Martin, T. Matzel, D. Maurin, S. W. McNutt, N. C. Mebus-Antunes, B. H. Meier, N. Meiser, M. Mompeán, E. Monaca, R. Montserret, L. Mariño Perez, C. Moser, C. Muhle-Goll, T. C. Neves-Martins, X. Ni, B. Norton-Baker, R. Pierattelli, L. Pontoriero, Y. Pustovalova, O. Ohlenschläger, J. Orts, A. T. Da Poian, D. J. Pypker, C. Richter, R. Riek, C. M. Rienstra, A. Robertson, A. S. Pinheiro, R. Sabbatella, N. Salvi, K. Saxena, L. Schulte, M. Schiavina, H. Schwalbe, M. Silber, M. da S Almeida, M. A. Sprague-Piercy, G. A. Spyroulias, S. Sreeramulu, J. N. Tants, K. Tãrs, F. Torres, S. Töws, M. Treviño, S. Trucks, A. C. Tsika, K. Varga, Y. Wang, M. E. Weber, J. E. Weigand, C. Wiedemann, J. Wirmer-Bartoschek, M. A. Wirtz Martin, J. Zehnder, M. Hengesbach, A. Schlundt, *Front. Mol. Biosci.* **2021**, *8*, 1–25.
- [20] D. R. Whelan, K. R. Bamberg, P. Heraud, M. J. Tobin, M. Diem, D. McNaughton, B. R. Wood, *Nucleic Acids Res.* **2011**, *39*, 5439–5448.
- [21] M. L. S. Mello, B. C. Vidal, *PLoS One* **2012**, *7*, 1–12.
- [22] H. Yang, S. Yang, J. Kong, A. Dong, S. Yu, *Nat. Protoc.* **2015**, *10*, 382–393.
- [23] D. M. Byler, H. Susi, *Biopolymers* **1986**, *25*, 469–487.
- [24] D. Roy, A. Chakraborty, R. Ghosh, *RSC Adv.* **2017**, *7*, 40563–40570.
- [25] M. Bouvet, I. Imbert, L. Subissi, L. Gluais, B. Canard, E. Decroly, *Proc. Natl. Acad. Sci. USA* **2012**, *109*, 9372–9377.
- [26] F. Ferron, L. Subissi, A. Theresa, S. De Moraes, N. Thi, T. Le, M. Sevajol, *Proc. Natl. Acad. Sci. USA* **2018**, *115*, E162–E171.

Manuscript received: September 15, 2021  
 Revised manuscript received: September 18, 2021  
 Accepted manuscript online: September 20, 2021  
 Version of record online: October 14, 2021